The SunCHECK™ Platform powers Quality Management in radiation therapy.

Scalable to meet the needs of any clinic or network, SunCHECK helps:

- **Reduce risks**
- **Control costs**
- **Improve treatment quality**

Visit sunnuclear.com to learn how SunCHECK fits into your clinic.

Patient Safety Starts Here

SUN NUCLEAR corporation

Feasibility of real-time motion management with helical tomotherapy

Eric Schnarr[a)], Matt Beneke, Dylan Casey, Edward Chao, Jonathan Chappelow, Andrea Cox, Doug Henderson, Petr Jordan, Etienne Lessard, Dan Lucas, Andriy Myronenko, and Calvin Maurer
Accuray Incorporated, 1310 Chesapeake Terrace, Sunnyvale, CA 94089, USA

(Received 13 September 2017; revised 21 December 2017; accepted for publication 11 January 2018; published 23 February 2018)

Purpose: This study investigates the potential application of image-based motion tracking and real-time motion correction to a helical tomotherapy system.
Methods: A kV x-ray imaging system was added to a helical tomotherapy system, mounted 90 degrees offset from the MV treatment beam, and an optical camera system was mounted above the foot of the couch. This experimental system tracks target motion by acquiring an x-ray image every few seconds during gantry rotation. For respiratory (periodic) motion, software correlates internal target positions visible in the x-ray images with marker positions detected continuously by the camera, and generates an internal–external correlation model to continuously determine the target position in three-dimensions (3D). Motion correction is performed by continuously updating jaw positions and MLC leaf patterns to reshape (effectively re-pointing) the treatment beam to follow the 3D target motion. For motion due to processes other than respiration (e.g., digestion), no correlation model is used — instead, target tracking is achieved with the periodically acquired x-ray images, without correlating with a continuous camera signal.
Results: The system's ability to correct for respiratory motion was demonstrated using a helical treatment plan delivered to a small (10 mm diameter) target. The phantom was moved following a breathing trace with an amplitude of 15 mm. Film measurements of delivered dose without motion, with motion, and with motion correction were acquired. Without motion correction, dose differences within the target of up to 30% were observed. With motion correction enabled, dose differences in the moving target were less than 2%.

Nonrespiratory system performance was demonstrated using a helical treatment plan for a 55 mm diameter target following a prostate motion trace with up to 14 mm of motion. Without motion correction, dose differences up to 16% and shifts of greater than 5 mm were observed. Motion correction reduced these to less than a 6% dose difference and shifts of less than 2 mm.
Conclusions: Real-time motion tracking and correction is technically feasible on a helical tomotherapy system. In one experiment, dose differences due to respiratory motion were greatly reduced. Dose differences due to nonrespiratory motion were also reduced, although not as much as in the respiratory case due to less frequent tracking updates. In both cases, beam-on time was not increased by motion correction, since the system tracks and corrects for motion simultaneously with treatment delivery. [https://doi.org/10.1002/mp.12791]

Key words: gating, internal–external correlation, intrafraction motion, organ motion, tomotherapy

1. INTRODUCTION

Targets move during radiotherapy treatment for many reasons, including bodily processes such as respiration and digestion. It is clinically beneficial to account for this motion, to ensure that the target receives the prescribed dose, as well as to minimize toxicity associated with irradiation of surrounding healthy tissue. Accounting for motion is particularly important when higher doses of radiation are delivered in fewer sessions than conventional radiotherapy, such as for stereotactic body radiation therapy (SBRT).

Various pretreatment and in-treatment approaches have been used to manage target motion. Pretreatment alternatives include expanding planning target volume (PTV) margins, immobilizing the patient or target, or both. Immobilization techniques include the use of deep inspiration breath-hold,[1] abdominal compression,[2] bladder and bowel preparation,[3] and other similar methods of physically limiting motion. But immobilization methods are generally inconvenient and negatively impact patient comfort. Margin expansion for respiratory motion is usually done through the definition of an internal target volume (ITV) that covers the target throughout its entire range of motion. Whether using an ITV for respiratory motion, or simply expanding PTV margins for other motion-related setup uncertainty, the resulting target volumes can be large and include additional healthy tissue. Furthermore, it has been shown that target motion can change substantially from day to day and even during treatment, which means that an ITV defined during treatment planning may not accurately cover the target range of motion during treatment delivery.[4]

In-treatment techniques focus on adjusting the treatment delivery to the patient, rather than forcing patient anatomy to

stay in the planned path of the treatment beam. This requires technology to track the target position and hardware capable of changing the planned treatment delivery to correct for the motion. For many radiotherapy systems, this means stopping treatment delivery when a motion larger than a specified threshold is detected, then repositioning the couch, and possibly acquiring additional images to verify the patient's position, before resuming treatment delivery.

In the case of targets that move with respiration, some radiotherapy systems gate the treatment delivery based on the patient's respiratory cycle, that is, these systems turn the radiation on only when the target is in the path of the treatment beam. Respiratory gating is time consuming, because the radiation is turned off for most of the respiratory cycle; the duty cycle is typically less than 30%. A wider gating window — the portion of the respiratory cycle during which radiation is turned on — not only results in faster treatment but also reduces the precision of delivery and results in more normal tissue being irradiated.[5]

Real-time motion compensation techniques go further and retarget the treatment beam to follow the moving target, without interrupting treatment delivery. The treatment beam moves as the target gradually drifts (common for intracranial and spine targets), unpredictably shifts (common for prostate and gynecological targets), or moves with respiration (common for abdominal and thoracic targets). This technique maintains delivery accuracy throughout treatment delivery and enables planning with minimal PTV margin expansion.[6–8] For targets that move with respiration, real-time re-targeting enables PTV margins similar to those used with very short gating windows, but without increasing delivery times (a 100% duty cycle).[9–13] The CyberKnife® System (Accuray Incorporated, Sunnyvale, CA, USA) is an example of a commercially available radiation therapy system that tracks a moving target and corrects for target motion in real-time.[14]

Helical tomotherapy systems, such as the Radixact™ Treatment Delivery System (Accuray Incorporated), provide precise treatments with conformal dose distributions,[15–18] but helical delivery modalities are incompatible with some forms of motion management. For example, the continuous gantry and couch motion of a helical delivery make it difficult to pause and resume a treatment and only treat during a breath-hold, let alone be fast enough to pause and resume for respiratory gating. However, real-time motion correction is compatible with the helical delivery modality. In this study, we describe how image-based motion tracking and real-time motion correction, similar to that performed by the CyberKnife system, can be applied to a helical tomotherapy system, and provide experimental results demonstrating its feasibility.

2. MATERIALS AND METHODS

2.A. The experimental system

Figure 1 shows the experimental system built to demonstrate the feasibility of real-time motion tracking and correction with helical tomotherapy. It is a functional helical tomotherapy delivery system, capable of delivering helical procedures. In addition to the standard functionality, the system also takes two-dimensional (2D) x-ray images with an EMD Epsilon kV x-ray generator, Dunlee DA1092 kV tube, and PerkinElmer 1642 flat-panel detector. The tube and detector are mounted 90 degrees offset from the MV beamline. Due to space limitations on this gantry, the generator is mounted to a metal plate on the back side of the gantry. A Boulder Innovation Group FP7000 optical camera (not shown) is installed above the foot of the couch, looking into the bore.

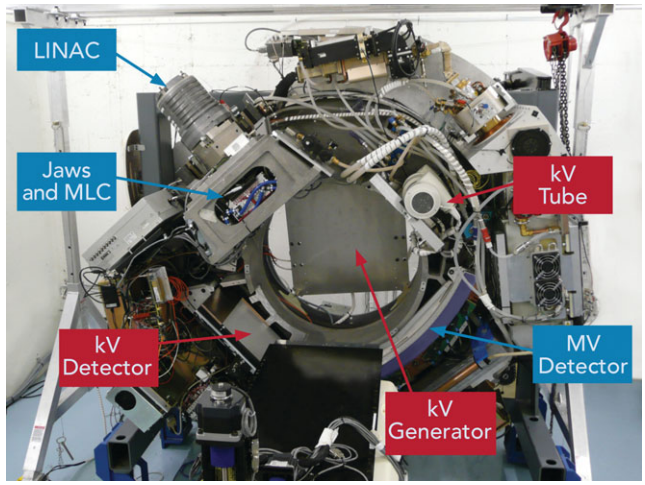

FIG. 1. A picture of the experimental tomotherapy system, highlighting the kV x-ray tube and detector mounted orthogonal to the MV beamline. The kV generator is mounted to a metal plate on the back side of the gantry. [Color figure can be viewed at wileyonlinelibrary.com]

The jaws and MLC, which normally collimate the treatment beam during treatment delivery, are adjusted in real-time to repoint the treatment beam and follow target motion. As the couch progressively moves into the gantry and the linear accelerator continuously rotates around the patient, the jaws are shifted to compensate for superior–inferior target motion (Fig. 2) and the planned leaf patterns are shifted left–right along the binary MLC to compensate for anterior–posterior and mediolateral motions (Fig. 3).

The experimental system's latency for respiratory motion correction is about 70 ms: (a) 10 ms latency comes from the optical camera running at 100 Hz; (b) It takes less than 10 ms to compute a 3D target position and transmit it to the embedded controller on the gantry; and (c) The MLC leaves take about 50 ms to physically transition between open and closed states. The jaws react more quickly (about 10 ms), so motion correction in the superior–inferior direction has an overall latency less than 30 ms. Because the latency is low (30 ms for jaws, 70 ms for MLC leaves), a simple linear extrapolation of the target motion based on the amplitude's rate of change was used to calculate jaw and leaf shifts.

2.B. Imaging during treatment

Figure 4 shows kV x-ray images of a pelvis phantom acquired on the experimental system, with the MV treatment

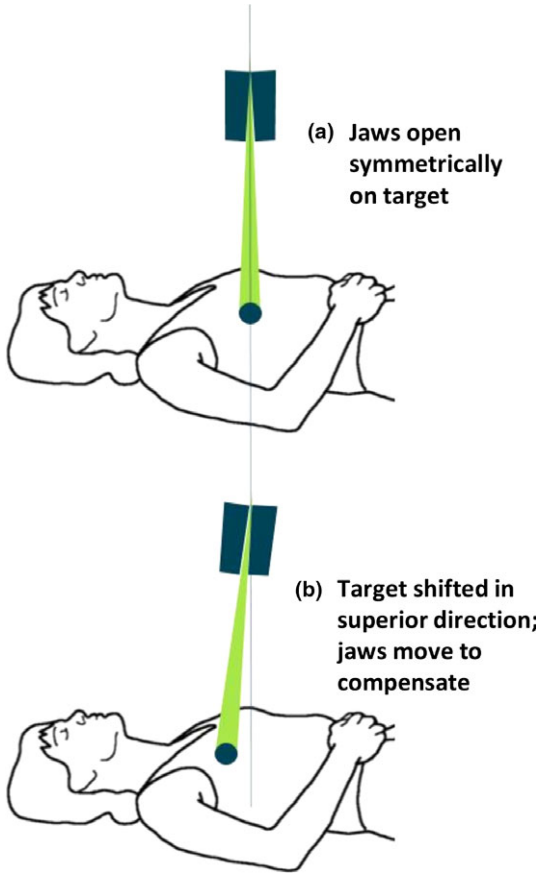

FIG. 2. Correction of the superior–inferior component of target motion: As the couch moves the patient into the gantry, the jaws move in the IEC-y direction to compensate for superior–inferior target motion. [Color figure can be viewed at wileyonlinelibrary.com]

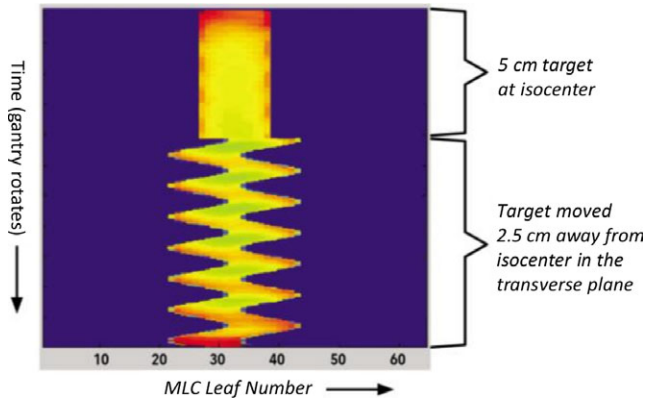

FIG. 3. Correction of the anterior–posterior and mediolateral components of target motion: As the couch moves into the gantry and the linear accelerator continuously rotates around the patient, the binary MLC shifts its open leaf pattern to compensate for target motion in the transverse plane. The leaf shifts follow a sinusoidal pattern due to gantry rotation around the patient. [Color figure can be viewed at wileyonlinelibrary.com]

beam off (left) and with the treatment beam on (right). The images were acquired at a gantry angle of −45°, with imaging settings of 125 kV, 30 mA, and 30 ms, which results in approximately 1 mGy of dose per image. Four gold fiducials are visible near the center of these images. Simulated pelvis and hip bones are also visible, as are a series of dowel pins (darker horizontal bands) and the gaps between phantom slabs (lighter vertical lines). A dark horizontal band in the upper half of the images is caused by the edge of the couch.

With the MV beam on, the image appears noisier and has subtle horizontal line artifacts that are not in the image with the MV beam off. Despite these differences, the four gold fiducials are clearly visible near the center of both images, and were used successfully by the software to track target position.

2.C. Sequential monoscopic imaging and tracking

The experimental system does not acquire simultaneous orthogonal x-ray images. Instead, individual images are taken by a single imager, several seconds apart as the gantry rotates. We call this *sequential monoscopic* imaging. Targets may move between image acquisitions, so 3D positions cannot be derived by simply triangulating their position from a pair of images. To handle this, the system builds a correlation model directly between breathing amplitude (measured with optical markers on the patient's chest or abdomen) and 2D positions detected in the x-ray images, without first deriving the 3D target positions. Equation (1) describes the basic least-squares minimization problem used to derive a 3D motion model:

$$\min_{f} \sum_{i=1}^{n} \sum_{j=1}^{m} \left\| P_{g_i,c_i}\left(f\left(a_i, \mathbf{s}_j\right)\right) - \mathbf{p}_{i,j} \right\|^2 \tag{1}$$

The motion model f is optimized such that the motion of fiducials inside the patient best matches the detected 2D fiducial locations in the x-ray images. The $\mathbf{p}_{i,j}$ are the 2D fiducial locations in the $i = 1\ldots n$ images, for $j = 1\ldots m$ fiducials. The motion model f is a function of the breathing amplitude a_i at the time of image i acquisition and 3D fiducial position $\mathbf{s}_j$, to a motion adjusted 3D position $\mathbf{s}'_j$. The function $P_{g_i,c_j}(\mathbf{s}'_j)$ projects the motion adjusted 3D position to its corresponding 2D position in the x-ray image, given gantry angle g_i and couch position c_i corresponding to image i.

The experimental system uses a fiducial detection algorithm adapted from CyberKnife to find the 2D fiducial locations ($\mathbf{p}_{i,j}$), then uses the Ceres Solver library (Google Inc., Mountain View, CA, USA) to solve for the motion model in the equation above. Running on the experimental system's operator console computer, the motion model takes less than 100 ms to calculate, but the 2D fiducial localization takes approximately 1 s, and so dominates the processing time. Once an optimal model function has been calculated, the 3D location of the target can be predicted for any breathing amplitude in just a few milliseconds. Let a be a breathing amplitude, and $\mathbf{t}$ be the 3D location of the target inside the patient without motion. Then the new 3D target location $\mathbf{t}'$ is simply:

$$\mathbf{t}' = f(a, \mathbf{t}) \tag{2}$$

Motion models can take a variety of forms. For example, linear motion is modeled as $f(a_i, \mathbf{s}_j) = [x_1, y_1, z_1]a_i + [x_2, y_2, z_2] + \mathbf{s}_j$. In this case, the minimization process must solve for six

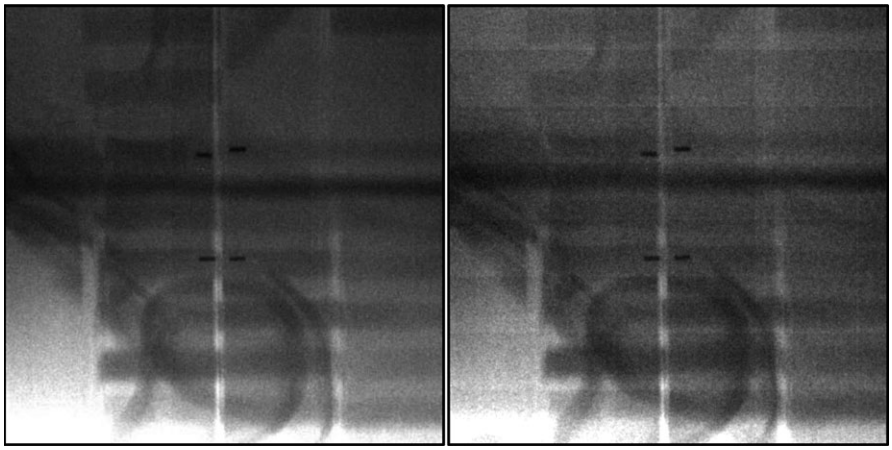

FIG. 4. Low dose (1 mGy) images of a pelvis phantom, with the treatment beam off (left) and with the treatment beam on (right). The images are cropped to focus on the region around the four gold fiducials used to track target position.

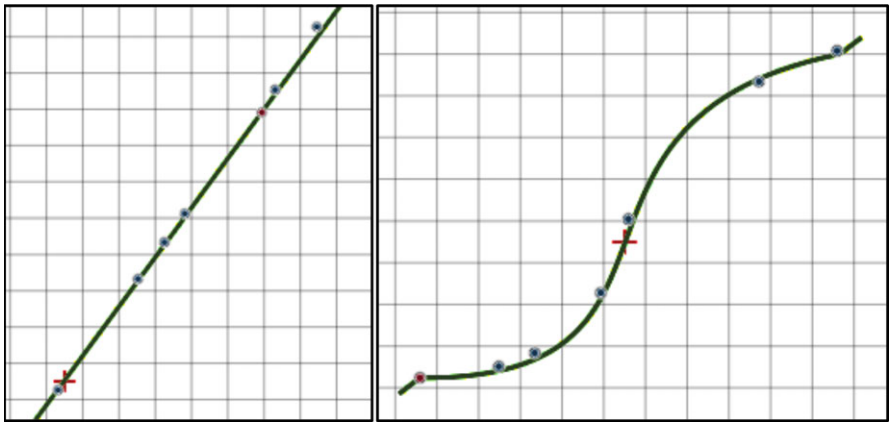

FIG. 5. A linear motion model (left) and cubic polynomial motion model (right) as they appear when projected to the flat-panel imager at a given gantry angle. The solid lines represent the continuous model function. The dots represent target locations detected in 2D on the flat-panel, and are inputs used to derive the model. [Color figure can be viewed at wileyonlinelibrary.com]

variables (x_1, x_2, y_1, y_2, z_1, z_1), and so requires a minimum of three flat-panel images to construct the model. Additional images can be used to improve the robustness and statistical confidence of the model. More complex motion paths can be modeled using alternate motion model formulae. For example, the model function could be a higher order polynomial (e.g., cubic) to handle nonlinear target motion, or a dual-polynomial to handle hysteresis, where motion during inhalation differs from motion during exhalation. Figure 5 illustrates possible linear and cubic motion models as they would appear when projected to the flat-panel imager for a given gantry angle. A motion model could also include rotation or even nonrigid spatial transforms. Models with more degrees of freedom require a greater minimum number of images to construct, and so require more additional images to reach the same level of robustness and statistical confidence as the linear model.

In practice, a patient's breathing pattern may not remain consistent over time. The system adapts to changes in breathing pattern by re-optimizing the model whenever a new image is acquired, taking about a second to process the image and update the model. Model adaptation is made more responsive to recent breathing changes by using only the n most recent images, and giving the more recent images more weight in the minimization objective function. In our formulation, weights are specified by increasing the expected error between the modeled versus predicted 2D locations, proportional to the age of the image.

Let σ represent the inherent accuracy of the 2D fiducial detection on the panel, for example, resulting from the finite pixel size and accuracy of the geometric alignment of the kV imaging components. Let σ' represent an expected rate of patient breathing pattern change over time, and $\Delta t_i = t_n - t_i$ be the time interval between the ith image and the most recent (nth) image, so $\Delta t_i \sigma'$ represents how much the breathing pattern in the ith image is expected to deviate from the current model. The motion model minimization formula, with aging, is given below:

$$\min_f \sum_{i=1}^{n} \sum_{j=1}^{m} \left[\frac{\left\| P_{g_i,c_i}\left(f\left(a_i, \mathbf{s}_j\right)\right) - \mathbf{p}_{i,j} \right\|}{\sigma + \Delta t_i \sigma'} \right]^2 \tag{3}$$

With the inclusion of aging, sequential monoscopic imaging can effectively track nonrespiratory motion as well as respiratory motion. The complication with

nonrespiratory motion is that there is no continuous external signal, like breathing amplitude, to correlate with the periodic x-ray images. The first indication the system has that motion has occurred is when the next x-ray image is acquired. Therefore, to be more responsive to target motion, the system must prefer position information derived from the most recent image.

To model nonrespiratory motion using the model optimization framework above, we first define the motion model function to be independent of breathing amplitude — for example, the function $f(a_i, \mathbf{s}_j) = [x, y, z] + \mathbf{s}_j$ models static translation of the 3D target and fiducial positions. Second, we optimize the model using only the most recent few images, typically as few as only two images ($n = 2$). Finally, the aging parameter (σ') is chosen to be consistent with the speed nonrespiratory targets are expected to move within the patient — for example, prostates have been observed to move slowly due to bladder filling throughout treatment. Now the model minimization process can accurately calculate the 3D position of stationary targets, and gracefully handle moving targets by preferring the position information from more recent images.

Our model minimization framework also provides a way to verify the consistency of the model. With stereoscopic imaging, it is possible to compare the positions detected along the axis shared by the two simultaneous images to verify the tracking result. This is not possible with sequential monoscopic imaging. Instead, we calculate model confidence as the probability that the optimized motion model is consistent with the 2D detected positions, given *a priori* expected detection accuracy (σ) and an image aging (σ') parameter. This probability is derived by calculating the area of the chi-squared distribution greater than the value of the optimized motion model. The degrees of freedom of the chi-squared distribution is two times the number of 2D images times the number of fiducials ($2mn$). The model confidence is shown mathematically in Eqs. (4) and (5) below.

$$\chi^2_{\text{opt}} = \sum_{i=1}^{n}\sum_{j=1}^{m}\left[\frac{\left\|P_{g_i,c_i}\left(f\left(a_i,\mathbf{s}_j\right)\right)-\mathbf{p}_{i,j}\right\|}{\sigma+\Delta t_i\sigma'}\right]^2 \tag{4}$$

$$\text{Model Confidence} = \Pr\left[\chi^2(2mn) > \chi^2_{\text{opt}}\right] \tag{5}$$

2.D. Experimental setup

Experiments were conducted by delivering helical tomotherapy treatment plans to a robotic phantom on the experimental motion management system. The treatment plans were created on a TomoTherapy® treatment planning system (Accuray Incorporated), and then exported to the experimental system. Clinically representative motion traces were used to drive the motion of the phantom: a respiratory amplitude trace collected from a CyberKnife System, and a 3D prostate motion trace collected using a Calypso® Extracranial Tracking System (Varian Medical Systems, Palo Alto, CA, USA).

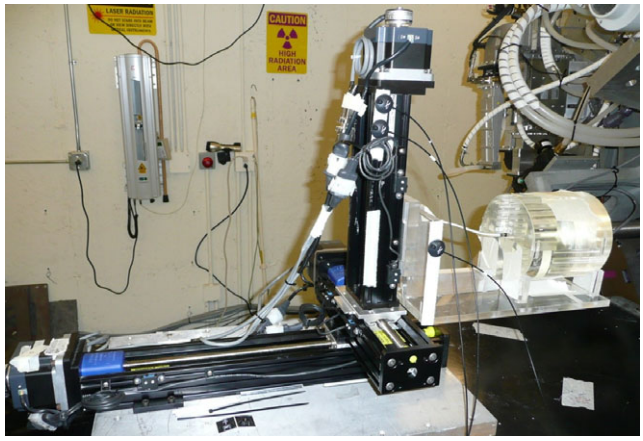

FIG. 6. A robotic phantom, developed in house to simulate target motion. [Color figure can be viewed at wileyonlinelibrary.com]

A custom designed robotic phantom, shown in Fig. 6, was used to simulate target motion. It consists of three linear actuators supporting an acrylic cylinder, which can hold a film and ion chamber to acquire dosimetric measurements. Gold fiducial markers — visible in kV x-ray images — were implanted inside the acrylic cylinder, and light-emitting diode (LED) markers visible to the optical camera were attached to the moving stage of the robotic platform. The phantom motion was synchronized to the start of procedure delivery, so the motion path could be reproduced exactly across multiple treatment deliveries.

Each treatment plan was delivered with three variations: (1) treatment delivery with no phantom motion, (2) treatment delivery with motion but no motion correction, and (3) treatment delivery with motion that was tracked and corrected for by the experimental system. Comparing variation 2 to variation 1 shows the impact of uncorrected motion. Comparing variation 3 to variation 2 shows how motion correction improves the delivered dose distribution. Phantom motion in the corrected and uncorrected variations was identical, so any measured differences are entirely attributable to the system's motion correction capability.

3. RESULTS

3.A. Respiratory motion experiment

To test the system's efficacy in correcting for respiratory motion, we delivered a helical tomotherapy treatment plan to a small moving target. A small target was chosen to exaggerate the dose differences resulting from motion, and make them more noticeable. The treatment plan was prescribed to cover a 10 mm diameter and 12 mm long cylindrical target to at least 2.5 Gy. It was planned using the 1.05 cm field width and a pitch of 0.28. The resulting treatment duration was 126 s, with a 16 s gantry period.

During delivery, the robotic phantom was programmed to move linearly, where all three axes followed the motion trace

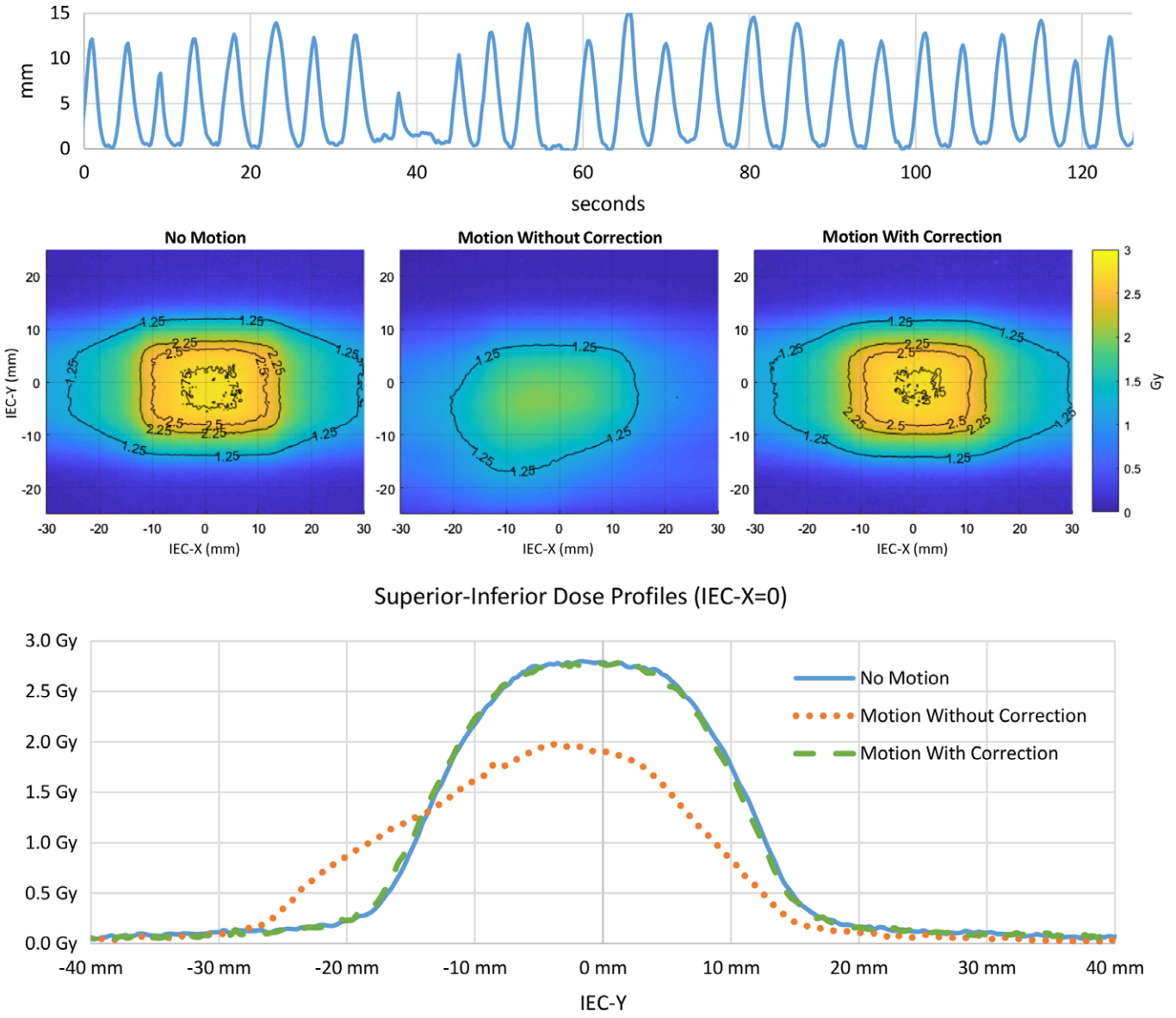

FIG. 7. Along the top is the respiratory motion trace used to drive the robotic phantom. In the middle are coronal films acquired with no motion (left), motion (center), and motion with correction (right). Isodose lines are overlaid on the films for 1.25 Gy (50% of the prescribed dose), 2.25 Gy (90%), 2.5 Gy (100%), and 2.75 Gy (110%). On the bottom are superior–inferior dose profiles (IEC-X = 0), with no motion (solid), motion without correction (dotted), and motion with correction (dashed). [Color figure can be viewed at wileyonlinelibrary.com]

shown at the top of Fig. 7. This motion trace has a maximum amplitude of approximately 15 mm, and is representative of a typical respiratory breathing pattern. Two x-ray images were acquired per rotation from −45 and +45 degrees, to detect the motion of a single fiducial located just superior of the target, and correlate it with the motion amplitude detected by the optical camera. The correlation model was then used to convert the optical camera signal into a new 3D target position every 10 ms.

Film measurements were acquired using Gafchromic™ EBT3 film (Ashland Advanced Materials, Bridgewater, NJ, USA) for the three delivery variations: no phantom motion, motion without correction, and motion with correction, as shown in Fig. 7. We observe that when no motion correction was applied the dose distribution was blurred out, had a lower peak dose, and was generally distorted because of the diagonal motion of the phantom. The peak dose was approximately 30% low compared to the reference with no phantom motion. When motion correction was enabled the corrected dose closely matched the reference dose, with less than 2% difference in peak dose, demonstrating the system's ability to correct for respiratory motion.

3.B. Prostate motion experiment

We also evaluated the system's ability to correct for non-respiratory motion, such as the gradual drift and unpredictable shifts that can occur in prostate treatments. In this

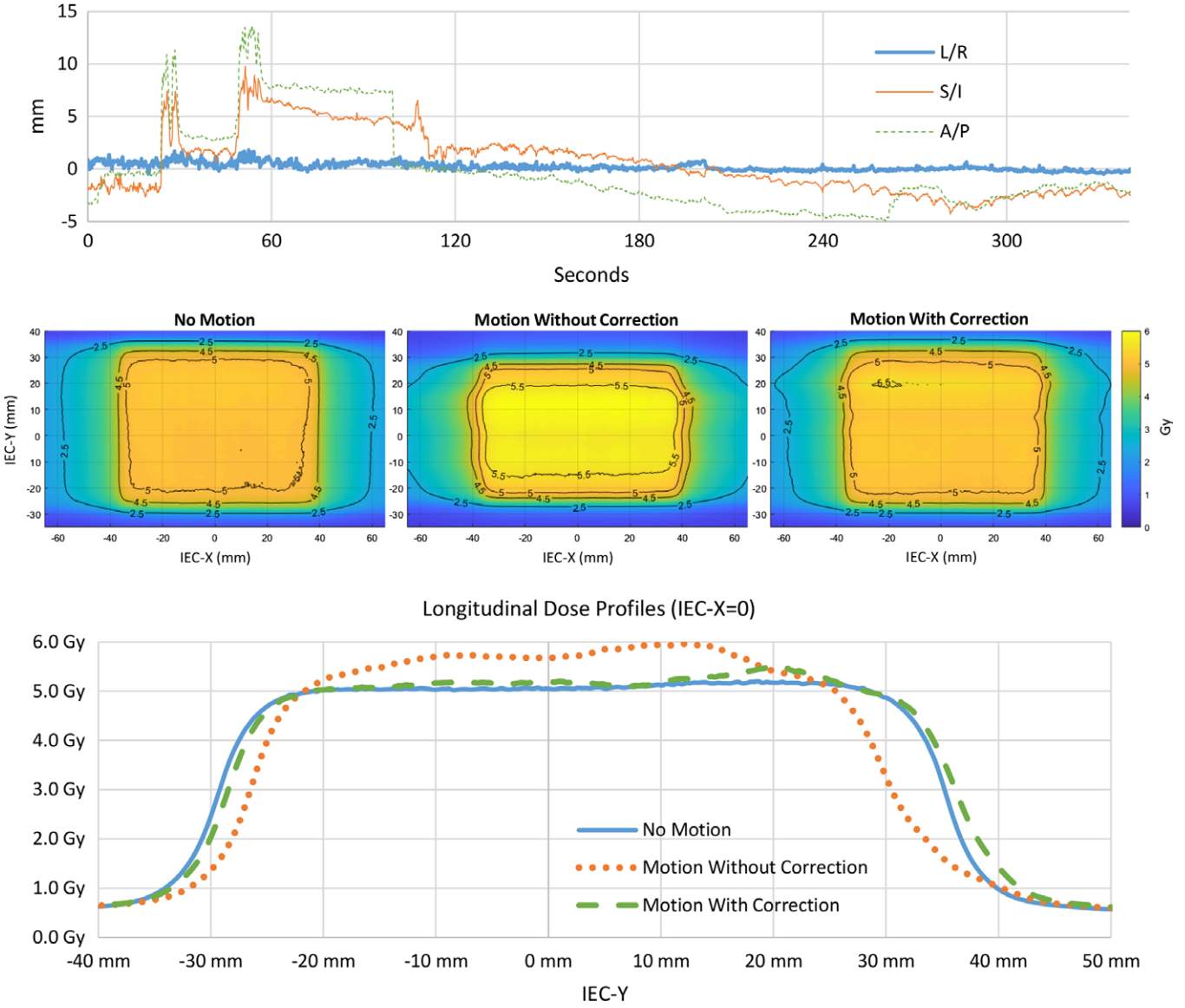

FIG. 8. Along the top is the prostate motion trace used to drive the robotic phantom, left–right motion (thick), superior–inferior (thin), and anterior–posterior (dashed). In the middle are coronal films acquired with no motion (left), motion (center), and motion with correction (right). Isodose lines are overlaid on the films for 2.5 Gy (50% of the prescribed dose), 4.5 Gy (90%), 5.0 Gy (100%), and 5.5 Gy (110%). On the bottom are superior–inferior dose profiles (IEC-X = 0), with no motion (solid), motion without correction (dotted), and motion with correction (dashed). [Color figure can be viewed at wileyonlinelibrary.com]

case, a plan simulating a simplified hypofractionated helical prostate treatment was used. The treatment plan was prescribed to cover a 60 mm diameter, 55 mm long cylindrical target to at least 5.0 Gy. It was planned using the 2.5 cm field width, and used the Dynamic Jaw Mode to produce sharp dose gradients at the inferior and superior ends of the target. The plan used a pitch of 0.12, resulting in a gantry period of 12 s and a total treatment duration of 336 s.

During delivery, the robotic phantom was programmed to reproduce a representative prostate motion trace, acquired from a patient using Calypso (see top of Fig. 8). The range of motion was −5 mm to +8 mm with intermittent excursions up to 14 mm. Two x-ray images were acquired per rotation from −45 and +45 degrees, corresponding to alternating intervals of 3 s and 9 s between image acquisitions, which matters because the optical camera is not used when tracking nonrespiratory motion.

The dose was measured using EDR2 film (Carestream Health, Rochester, NY, USA), and the results are shown in Fig. 8. We observe that when no motion correction is applied the dose is notably different from the reference dose with no phantom motion. The dose profile central region is hotter by up to 16%, and the superior and inferior ends are shifted toward the middle by 5 mm and 3 mm, respectively. When motion correction is enabled the dose more closely matches the reference, with a 6% difference in peak dose and less than a 2 mm shift at the superior and inferior ends. This demonstrates the system's ability to partially correct for motion with gradual drift and intermittent excursions.

The limiting factor in this case was the frequency of tracking updates. Unlike respiratory motion tracking, where the optical camera provides a continuous signal, new target position information is only available from periodic x-ray images. In this case, two images were acquired per rotation, 90 degrees apart, and the interval between image acquisitions alternated between 3 s and 9 s. Motion that occurred between acquisitions was not corrected for, and resulted in the observed residual delivery inaccuracy. More frequent imaging could improve the system's ability to correct for nonrespiratory motion.

4. DISCUSSION

The design of the experimental system is intentionally like that of the CyberKnife System: Both acquire periodic x-ray images to determine internal target location, correlate it with a continuous signal from an optical camera, and repoint the treatment beam in real-time to correct for target motion. In this study, we focused on tracking implanted fiducials, combined with respiratory motion (for targets like lung tumors) and nonrespiratory motion (for targets like the prostate). CyberKnife supports several additional tracking methods that could be adapted to helical tomotherapy, including skull, spine, and lung tumor tracking, all without using implanted fiducial markers. The submillimeter accuracy of these tracking methods on CyberKnife has been demonstrated and reported in the literature for both respiratory[11,13,19] and aperiodic nonrespiratory[20,21] motion targets, and we expect they would have similar performance on a helical tomotherapy system.

Treatment beam-on time is not increased by the system: x-ray images are acquired while the treatment beam is on, and so do not interrupt treatment delivery. Along with real-time motion correction via the jaws and MLC, this means that the treatment need not be interrupted and beam-on time is not increased when performing motion correction. In comparison to respiratory gating, our system can be said to have a 100% duty cycle.

Because only one kV x-ray imaging system is mounted on the gantry, motion tracking is accomplished by sequential monoscopic imaging, rather than by stereoscopic imaging. The methods for turning 2D locations in the sequential x-ray images into 3D target locations in the patient, or into a 3D amplitude-to-target correlation model for respiratory motion, are described in Section 2.C. In some ways, sequential monoscopic tracking is better than tracking with simultaneous image pairs, because the position information along a simultaneous image pair's shared axis is redundant: It can be used for error checking, but only provides three independent observations per image pair (1.5 independent observations per image). Sequential monoscopic images also have a shared axis but are acquired at different times, so each image provides two independent observations, and a robust motion model can be built from fewer images.

The lack of redundant information makes verifying tracking results more difficult, although similar functionality can be provided by a statistical confidence metric, as described in Section 2.C. When the optimized model is a good fit for the detected 2D fiducial locations, the confidence is high, generally near 100%. When something goes wrong with target tracking (e.g., a fiducial is misidentified in an x-ray image, resulting in a bad 2D position) then the confidence falls precipitously. And when 2D target tracking is working but the 3D motion is simply not well modeled (e.g., nonlinear target motion not modeled by a linear function) then the confidence decreases relative to how much the measured data deviates from the model. The user could set a threshold on model confidence below which the system would automatically pause the delivery, and catch 2D tracking errors and atypical target motion that is not modeled accurately.

Experimental results show the system is effective at correcting for respiratory motion, when the motion has a linear correlation with an external marker. In clinical practice, tumors sometimes follow more complex motion paths, so nonlinear motion models may be necessary for those cases. Synchrony Respiratory Tracking on CyberKnife includes multiple model types to handle linear and nonlinear target motion, and these model types could be adapted for use with sequential monoscopic imaging.

For nonrespiratory motion, published studies on intrafraction prostate motion show that rapid motions of several millimeters may be uncommon but do occur in practice.[22–24] Our results indicate that the delay between tracking updates, where motion of the target between image acquisitions goes uncorrected for several seconds, is a source of residual error when correcting for nonrespiratory motion.

This error could be reduced by imaging more frequently. For example, the system could rotate faster to reduce the time between images. Alternatively, it could acquire more images per rotation. Most kV x-ray imaging dose is deposited near the surface where the beam enters the patient, and the surface area irradiated by the imaging beam is small, so the system could take more images per rotation without increasing the peak imaging dose received by the patient. For example, the system could acquire four images per rotation at 90 degree intervals, and so acquire a new image every 3 s, assuming a 12 s gantry period. The imaging frequency could be selectable: In most patient plans, two images per rotation may be sufficient to track and correct for motion. In patient plans that are more sensitive to uncorrected motion, or for fractions where movement is more frequent, the imaging frequency could be increased as needed.

The dose distributions demonstrated by the experimental system are consistent with a previous motion correction simulation study performed by Price, et al.[25] using 4D dose calculation software. They reported, "When the jaw and MLC compensation program was engaged, the motion compromised PTV coverage was recovered back to >95% for all cases and plans." Their study included both lung and prostate cases, and their results for lung motion were similar to ours. For prostate cases, our results are not as good, because their study assumed motion correction was applied immediately after the target moved, whereas our results include the delay caused by periodic imaging.

5. CONCLUSIONS

This experimental work demonstrates the feasibility of image guided motion tracking and real-time motion correction on a helical tomotherapy system. Dose differences due to a simple respiratory motion profile were greatly reduced, and dose differences due to nonrespiratory motion were also reduced, although not as much as in the respiratory case due to less frequent tracking updates. In both cases, treatment beam-on time was not increased by using motion correction, since the system tracks and corrects for motion in real-time, simultaneous with treatment delivery.

ACKNOWLEDGMENTS

We thank Bill Butrymowicz, Yu Chen, Melissa Cooper, Joseph Homp, Thomas Kammeyer, Scott Lai, Carl Mauer, Tim Miller, Rob O'Connell, Ken Ruchala, and Robert Sinklair for their help in the development of the experimental system and their many contributions over the course of this project. We also thank Jun Lian of the University of North Carolina for sharing the Calypso trace used in our prostate motion experiment.

CONFLICTS OF INTEREST

This proof of concept study was performed by Accuray Incorporated, maker of the CyberKnife, TomoTherapy, and Radixact Treatment Delivery Systems. All the authors are Accuray employees.

[a)]Author to whom correspondence should be addressed. Electronic mail: eschnarr@accuray.com; Telephone: +608 824 2819.

REFERENCES

1. Latty D, Stuart KE, Wang W, Ahern V. Review of deep inspiration breath-hold techniques for the treatment of breast cancer. *J Med Radiat Sci*. 2015;62:74–81.
2. Negoro Y, Nagata Y, Aoki T, et al. The effectiveness of an immobilization device in conformal radiotherapy for lung tumor: reduction of respiratory tumor movement and evaluation of the daily setup accuracy. *Int J Radiat Oncol Biol Phys*. 2001;50:889–898.
3. Yahya S, Zarkar A, Southgate E, Nightingale P, Webster G. Which bowel preparation is best? Comparison of a high-fibre diet leaflet, daily microenema and no preparation in prostate cancer patients treated with radical radiotherapy to assess the effect on planned target volume shifts due to rectal distension. *Br J Radiol*. 2013;86:20130457.
4. Minn AY, Schellenberg D, Maxim P, et al. Pancreatic tumor motion on a single planning 4D-CT does not correlate with intrafraction tumor motion during treatment. *Am J Clin Oncol*. 2009;32:364–368.
5. Jiang SB. Technical aspects of image-guided respiration-gated radiation therapy. *Med Dosim*. 2006;31:141–151.
6. Xie Y, Djajaputra D, King CR, Hossain S, Ma L, Xing L. Intrafractional motion of the prostate during hypofractionated radiotherapy. *Int J Radiat Oncol Biol Phys*. 2008;72:236–246.
7. Van de Water S, Valli L, Aluwini S, Lanconelli N, Heijmen B, Hoogeman M. Intrafraction prostate translations and rotations during hypofractionated robotic radiation surgery: dosimetric impact of correction strategies and margins. *Int J Radiat Oncol Biol Phys* 2012; 88:1154–1160.
8. Hoogeman MS, Nuyttens JJ, Levendag PC, Heijmen BJ. Time dependence of intrafraction patient motion assessed by repeat stereoscopic imaging. *Int J Radiat Oncol Biol Phys*. 2008;70:609–618.
9. Yoon K, Kwak J, Cho B, et al. Gated volumetric-modulated arc therapy vs. tumor-tracking CyberKnife radiotherapy as stereotactic body radiotherapy for hepatocellular carcinoma: a dosimetric comparison study focused on the impact of respiratory motion managements. *PLoS ONE*. 2016;11:e0166927.
10. Rault E, Lacornerie T, Dang HP, et al. Accelerated partial breast irradiation using robotic radiotherapy: a dosimetric comparison with tomotherapy and three-dimensional conformal radiotherapy. *Radiat Oncol*. 2016;11:29.
11. Hoogeman MS, Prevost JB, Nuyttens J, Poll J, Levendag P, Heijmen B. Clinical accuracy of the respiratory tumor tracking system of the CyberKnife: assessment by analysis of log files. *Int J Radiat Oncol Biol Phys*. 2009;74:297–303.
12. Korreman SS, Juhler-Nottrup T, Boyer AL. Respiratory gated beam delivery cannot facilitate margin reduction, unless combined with respiratory correlated image guidance. *Radiother Oncol*. 2008;86: 61–68.
13. Seppenwoodle Y, Berbeco RI, Nishioka S, Shirato H, Heijmen B. Accuracy of tumor motion compensation algorithm from a robotic respiratory tracking system: a simulation study. *Med Phys*. 2007;34:2774–2784.
14. Kilby W, Dooley J, Kuduvalli G, Sayeh S, Maurer CR. The CyberKnife robotic radiosurgery system in 2010. *Technol Cancer Res Treat*. 2010;9:433–452.
15. Welsh JS, Patel RR, Ritter MA, Harari PM, Mackie TR, Mehta MP. Helical tomotherapy: an innovative technology and approach to radiation therapy. *Technol Cancer Res Treat*. 2002;1:311–316.
16. Fenwick JD, Tomé WA, Soisson ET, Mehta MP, Mackie TR. Tomotherapy and other innovative IMRT delivery systems. *Semin Radiat Oncol*. 2006;16:199–208.
17. Hodge W, Tomé WA, Jaradat HA, et al. Feasibility report of image guided stereotactic body radiotherapy (IG-SBRT) with tomotherapy for early stage medically inoperable lung cancer using extreme hypofractionation. *Acta Oncol*. 2006;45:890–896.
18. Sharma DS, Gupta T, Jalali R, Master Z, Phurailatpam RD, Sarin R. High-precision radiotherapy for craniospinal irradiation: evaluation of three-dimensional conformal radiotherapy, intensity-modulated radiation therapy and helical TomoTherapy. *Br J Radiol*. 2009;82:1000–1009.
19. Nioutsikou E, Seppenwoodle Y, Symonds-Tayler JR, Heijmen B, Evans P. Dosimetric investigation of lung tumor motion compensation with a robotic respiratory tracking system: an experimental study. *Med Phys*. 2008;35:1232–1240.
20. Drexler C, Furweger C. Quality assurance of a robotic, image guided radiosurgery system. WC 2009. IFMBE Proceedings 25/I; 2009:492–495.
21. Antypas C, Pantelis E. Performance evaluation of a CyberKnife G4 image-guided robotic stereotactic radiosurgery system. *Phys Med Biol*. 2008;53:4697–4718.
22. Kitamura K, Shirato H, Seppenwoolde Y, et al. Three-dimensional intrafractional movement of prostate measured during real-time tumor-tracking radiotherapy in supine and prone treatment positions. *Int J Radiat Oncol Biol Phys*. 2002;53:1117–1123.
23. Litzenberg DW, Balter JM, Hadley SW, et al. Influence of intrafraction motion on margins for prostate radiotherapy. *Int J Radiat Oncol Biol Phys*. 2006;65:548–553.
24. Willoughby TR, Kupelian PA, Pouliot J, et al. Target localization and real-time tracking using the Calypso 4D localization system in patients with localized prostate cancer. *Int J Radiat Oncol Biol Phys*. 2006;65:528–534.
25. Price A, Chao E, Chang S, Matney J, Wang A, Lian J. Intrafractional Motion Effect Can Be Minimized in Tomotherapy Stereotactic Body Radiotherapy (SBRT). AAPM 58th Annual Meeting; 2016. MO-FG-BRA-7.